

## Microstructural, electrical, and ferroelectric properties of $M_{0.5}\text{Bi}_{4.5-x}\text{Sm}_x\text{Ti}_4\text{O}_{15}$ ( $M = \text{Na}$ or $\text{K}$ ) thin films

Min Hwan Kwak<sup>a</sup>, Chinnambedu Murugesan Raghavan<sup>b</sup>, Sang Su Kim<sup>b</sup> and Won-Jeong Kim<sup>b,\*</sup>

<sup>a</sup>Department of Electrical Engineering, Changwon Moonsung University, Gyeongnam 51410, Korea

<sup>b</sup>Department of Physics, Changwon National University, Gyeongnam 51140, Korea

Aurivillius type  $M_{0.5}\text{Bi}_{4.5-x}\text{Sm}_x\text{Ti}_4\text{O}_{15}$  ( $x = 0$  and  $0.5$ ,  $M = \text{Na}$  or  $\text{K}$ ) thin films were prepared on Pt(111)/Ti/Si/SiO<sub>2</sub>(100) substrates by using a chemical solution deposition method. Fabricated thin films were crystallized in pure Aurivillius phase orthorhombic structures, which were confirmed by X-ray diffraction and Raman spectroscopy studies. The use of Sm<sup>3+</sup>-ions for doping purposes results in remarkable improvements in electrical and ferroelectric properties of the  $M_{0.5}\text{Bi}_{4.5-x}\text{Sm}_x\text{Ti}_4\text{O}_{15}$  thin films. A study of the ferroelectric hysteresis loops enabled the remnant polarization ( $2P_r$ ) and coercive field ( $2E_c$ ) values for the  $\text{Na}_{0.5}\text{Bi}_4\text{Sm}_{0.5}\text{Ti}_4\text{O}_{15}$  and the  $\text{K}_{0.5}\text{Bi}_4\text{Sm}_{0.5}\text{Ti}_4\text{O}_{15}$  thin films to be measured as 34.4 mC/cm<sup>2</sup> and 220 kV/cm at an applied electric field of 475 kV/cm and 36.0 mC/cm<sup>2</sup> and 103 kV/cm at 231 kV/cm, respectively. The  $2P_r$  values measured for the thin films doped with Sm<sup>3+</sup>-ions were much larger than those of the un-doped thin films. The  $2E_c$  values of the  $M_{0.5}\text{Bi}_{4.5-x}\text{Sm}_x\text{Ti}_4\text{O}_{15}$  thin films were also drastically lowered. Furthermore, low leakage current densities were measured for the  $M_{0.5}\text{Bi}_{4.5-x}\text{Sm}_x\text{Ti}_4\text{O}_{15}$  thin films.

**Key words:** Thin films, Electrical properties, Ferroelectric materials, X-ray methods.

### Introduction

Aurivillius phase bismuth layer-structured ferroelectric (BLSF) compounds, which have the general formula  $(\text{Bi}_2\text{O}_2)^{2+}(\text{A}_{n-1}\text{B}_n\text{O}_{3n+1})^{2-}$ , have gained enormously in technological importance because of their ferroelectric and piezoelectric behavior [1-6]. In the chemical formula,  $A$  can be a mono-, bi-, or tri- valence ion, allowing dodecahedral co-ordination, and  $B$  can be a tetra-, penta- or hexa-valence transition metal ion, allowing octahedral co-ordination within an orthorhombic structure. The integer  $n$  is the number of  $\text{BO}_6$  octahedra in the pseudo-perovskite block of BLSFs. These compounds are built-up by the regular inter-growth of  $(\text{Bi}_2\text{O}_2)^{2+}$  layers and pseudo-perovskite  $(\text{A}_{n-1}\text{B}_n\text{O}_{3n+1})^{2-}$  layers along the  $c$ -axis<sup>3-7</sup>. BLSFs are suggested to be a good idea for the fabrication of nonvolatile ferroelectric random-access memory devices owing to their superior fatigue-free nature [1, 8-10].

Aurivillius BLSF  $M_{0.5}\text{Bi}_{4.5}\text{Ti}_4\text{O}_{15}$  ( $M = \text{Na}$  or  $\text{K}$ ) ( $n = 4$ ) compounds have recently attracted special interest among researchers owing to their superior piezoelectric and ferroelectric properties [4, 5, 10, 11].  $M_{0.5}\text{Bi}_{4.5}\text{Ti}_4\text{O}_{15}$  ( $M = \text{Na}$  or  $\text{K}$ ) compounds have several advantages, including a stable crystal structure, high ferroelectric phase-transition temperature, high piezoelectric coefficient with

large mechanical quality factor, and nontoxic lead-free nature [10-16]. The ferroelectric phase transition temperatures for the  $\text{Na}_{0.5}\text{Bi}_{4.5}\text{Ti}_4\text{O}_{15}$  (NaBTi) and the  $\text{K}_{0.5}\text{Bi}_{4.5}\text{Ti}_4\text{O}_{15}$  (KBTi) thin films have been reported to be 655 °C and 550 °C, respectively [7]. However, there are a few major problems associated with  $M_{0.5}\text{Bi}_{4.5}\text{Ti}_4\text{O}_{15}$  ( $M = \text{Na}$  or  $\text{K}$ ) compounds. Particularly, the preparation of the pure phase of these compounds is quite difficult because of the volatile nature of the Na, K, and Bi-ions [11]. The formation of secondary phases leads to a large leakage current in these compounds. To solve the above problem, the addition of excessive amounts of Na, K, and Bi-ions has been suggested to maintain the stoichiometry in these compounds [17]. In thin film form, the  $M_{0.5}\text{Bi}_{4.5}\text{Ti}_4\text{O}_{15}$  ( $M = \text{Na}$  or  $\text{K}$ ) compounds were often found to show low remnant polarization, which is considered to be another major problem with the use of these compounds in ferroelectric devices [11]. In order to enhance the ferroelectric properties, doping the Bi-site of BLSFs with rare-earth (RE) lanthanide ions, such as La<sup>3+</sup>, Nd<sup>3+</sup>, Sm<sup>3+</sup>, and Pr<sup>3+</sup> has been strongly recommended [2, 9, 18, 19]. Incorporation of an RE metal ion into the Bi-site of BLSFs is able to induce structural distortion, which is deemed to be more beneficial for enhancing the ferroelectric polarization. Furthermore, doping with RE metal ions has a tendency to reduce the concentration of oxygen vacancies in BLSFs.

Among the lanthanides, the Sm<sup>3+</sup>-ion has been reported to be more appropriate for incorporation into the Bi-site of BLSFs [18, 19]. Cohn *et al.* reported

\*Corresponding author:  
Tel : +82-55-213-3428  
Fax: +82-55-267-0264  
E-mail: kwj@changwon.ac.kr

tremendously enhanced ferroelectric polarization for the  $\text{Bi}_{4-x}\text{Sm}_x\text{Ti}_3\text{O}_{12}$  thin film [18]. Doping with the  $\text{Sm}^{3+}$ -ion stabilizes the pseudo-perovskite phase in the BLSF structure. Due to the similarity of the ionic radius of  $\text{Sm}^{3+}$ -ion (1.00 Å) and  $\text{Bi}^{3+}$ -ion (0.93 Å), Sm atoms are easily replace Bi atoms in the the BLSFs. Furthermore, the transition temperature of the  $\text{Sm}^{3+}$ -doped BLSFs is sufficiently high for ferroelectric applications [18]. To the best of our knowledge, there are no reports on the effect of  $\text{Sm}^{3+}$ -ion doping on the properties of  $M_{0.5}\text{Bi}_{4.5}\text{Ti}_4\text{O}_{15}$  ( $M = \text{Na}$  or  $\text{K}$ ) thin films. In this study, we have investigated the effects of  $\text{Sm}^{3+}$ -ion doping on the microstructural, electrical, and ferroelectric properties of the  $M_{0.5}\text{Bi}_{4.5}\text{Ti}_4\text{O}_{15}$  ( $M = \text{Na}$  or  $\text{K}$ ) thin films, which were prepared by using a chemical solution deposition (CSD) method.

### Experimental Procedure

$M_{0.5}\text{Bi}_{4.5-x}\text{Sm}_x\text{Ti}_4\text{O}_{15}$  ( $x = 0$  and  $0.5$ ,  $M = \text{Na}$  and  $\text{K}$ ) thin films were prepared on Pt(111)/Ti/SiO<sub>2</sub>/Si(100) substrates by using a CSD method. Sodium nitrate [ $\text{NaNO}_3$ ], potassium nitrate [ $\text{KNO}_3$ ], bismuth nitrate pentahydrate [ $\text{Bi}(\text{NO}_3)_3 \cdot 5\text{H}_2\text{O}$ ], samarium nitrate hexahydrate [ $\text{Sm}(\text{NO}_3)_3 \cdot 6\text{H}_2\text{O}$ ], and titanium isopropoxide [ $\text{Ti}[\text{OCH}(\text{CH}_3)_2]_4$ ] were used as starting materials to prepare precursor solutions. 2-Methoxy ethanol (2-MOE) was used as solvent, and acetic acid was used as catalyst. For the preparation of the  $M_{0.5}\text{Bi}_{4.5-x}\text{Sm}_x\text{Ti}_4\text{O}_{15}$  ( $x = 0$  and  $0.5$ ,  $M = \text{Na}$  or  $\text{K}$ ) precursor solutions, sodium nitrate or potassium nitrate was dissolved in the 2-MOE solvent at 40 °C, and stirred for 30 min, then acetic acid as catalyst was added to the above solution and stirred for another 30 min to attain homogenization. Bismuth nitrate pentahydrate and samarium nitrate hexahydrate were added to the above solution mixture and stirred for another 30 min. To maintain the stoichiometric compositions of the films, 15% excess concentrations of Na, K, and Bi ions have been used. Both Na-Bi-Sm and K-Bi-Sm solutions were stirred for an extra 2 h to make homogeneous solutions. Separately, titanium isopropoxide added solution of 2-MOE and acetyl acetone was prepared in a glove box and stirred for 1.5 h. Ti-solution was mixed with the Na-Bi-Sm and the K-Bi-Sm solutions, respectively, to form the  $\text{Na}_{0.5}\text{Bi}_4\text{Sm}_{0.5}\text{Ti}_4\text{O}_{15}$  (NaBSmTi) and the  $\text{K}_{0.5}\text{Bi}_4\text{Sm}_{0.5}\text{Ti}_4\text{O}_{15}$  (KBSmTi) precursor solutions. The resulting solution mixtures were continuously stirred for 3 h to attain homogenization. The same method was used to prepare pure NaBTi and KBTi precursors to fabricate NaBTi and KBTi films without Sm dopants. The final concentrations of these solutions were adjusted to 0.1M.

The NaBTi, NaBSmTi, KBTi, and KBSmTi precursor solutions were spin-coated onto Pt(111)/Ti/SiO<sub>2</sub>/Si(100) substrates at an angular speed of 3000 rpm for 20 s. The deposited wet thin layers were prebaked at 200 °C and 360 °C for 5 min on a hot plate to dry as well as to

eliminate organic impurities. Both coating and baking processes were repeated 15 times to make thick films. Finally, the multiple coated layers were annealed twice at 500 °C and 700 °C for 3 min for each by rapid thermal annealing (RTA) with oxygen flow.

The structures of the  $M_{0.5}\text{Bi}_{4.5-x}\text{Sm}_x\text{Ti}_4\text{O}_{15}$  ( $x = 0$  and  $0.5$ ,  $M = \text{Na}$  or  $\text{K}$ ) thin films were investigated by using an X-ray diffractometer (Rigaku, MiniFlex II) with a copper target and a Raman spectroscopy (Jasco, NRS-3100). The surface morphologies and the thicknesses of the thin films were examined by using a field emission scanning electron microscope (Tescan, MIRA II LMH). For the electrical and the ferroelectric measurements, platinum electrodes with areas of  $1.54 \times 10^{-4} \text{ cm}^2$  were deposited on the top of thin films by ion sputtering using a metallic shadow mask. The ferroelectric hysteresis was measured by using a standardized ferroelectric test system (Radiant Technologies Inc., Precision LC). The dielectric properties and the leakage current densities of the fabricated thin films were measured by using a low-frequency impedance analyzer (HP, 4192A) and an electrometer (Keithley, 6517A), respectively.

### Results and Discussion

Fig. 1 shows the X-ray diffraction (XRD) patterns of the NaBTi, KBTi, NaBSmTi, and KBSmTi thin films fabricated on Pt(111)/Ti/SiO<sub>2</sub>/Si(100) substrates by using a CSD method. It has been found that the films were crystallized in the pure phases of the Aurivillius structures. The XRD peaks were indexed as polycrystalline orthorhombic ( $A2_1am$ ). From Fig. 1, it is obvious that  $\text{Sm}^{3+}$ -ions doping on the Bi-site of  $M_{0.5}\text{Bi}_{4.5}\text{Ti}_4\text{O}_{15}$  ( $M = \text{Na}$  or  $\text{K}$ ) does not significantly influence the original Aurivillius structures. However, there are slight changes in the diffraction peaks of (119), (0016), and (020)/(200) in peaks of the

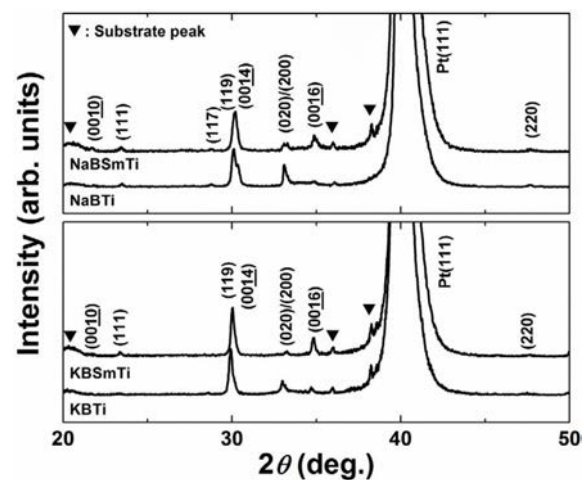
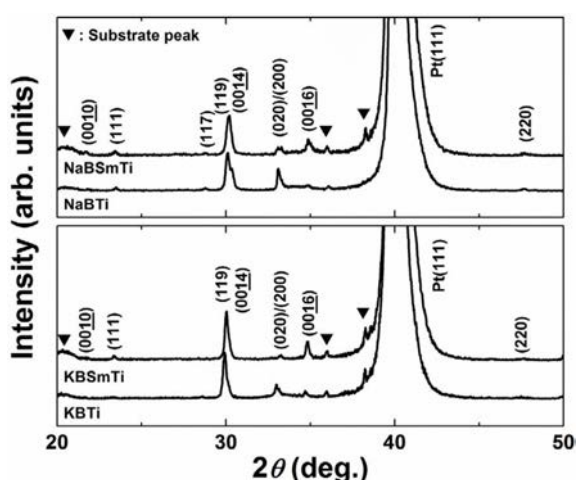


Fig. 1. XRD patterns of the NaBTi, KBTi, NaBSmTi, and KBSmTi thin films deposited on Pt(111)/Ti/SiO<sub>2</sub>/Si(100) substrates.



**Fig. 2.** Raman scattering spectra with the fitted curves (thick solid lines) and their decomposed active modes (thin solid lines) of the NaBTi, KBTi, NaBSmTi, and KBSmTi thin films.

NaBSmTi and the KBSmTi thin films when compared with both NaBTi and KBTi thin films. The (119) peak was shifted to a slightly higher angle in both NaBSmTi and KBSmTi thin films. The (0016) peak of the  $Sm^{3+}$ -ion doped thin films was quite intense. The intensities of the (020)/(200) peaks were relatively low in the NaBSmTi and the KBSmTi thin films. These small changes observed for the NaBSmTi and the KBSmTi thin films can be related to internal strain in the Aurivillius structures caused by  $Sm^{3+}$ -ion doping.

The effects of  $Sm^{3+}$ -ion doping on both NaBTi and KBTi thin films were further investigated by Raman scattering spectroscopy studies. The Raman scattering spectra of the NaBTi, NaBSmTi, KBTi, and KBSmTi thin films, which were recorded at room temperature by using a solid-state laser of wavelength 532 nm, are shown in Fig. 2. The Raman active modes were estimated precisely by fitting and decomposing the measured Raman spectra as shown in Fig. 2. The Raman spectra recorded for the films are match well with the typical Raman spectra of the BLSF structures reported throughout the literature [20-22]. Typically, the Raman modes of BLSF structures occur because of internal vibrations in the  $TiO_6$  octahedra as well as lattice transitions caused by the cationic motions in the pseudo-perovskite blocks [21]. The Raman spectra of the BLSF compounds are generally classified into two active spectral regions, in which the phonon modes

formed in the low-frequency region ( $\sim 90$  to  $\sim 200$   $cm^{-1}$ ) are caused by the vibrations of the  $A$ -site ions in the pseudo-perovskite block and the Raman modes in the high-frequency region (above  $200$   $cm^{-1}$ ) are related to the stretching and the bending vibrations of the  $TiO_6$  octahedra in the pseudo-perovskite block [21, 22]. Observed Raman modes for the NaBTi, NaBSmTi, KBTi, and KBSmTi films are presented in Table 1, where the Raman modes below  $200$   $cm^{-1}$  are related to the internal vibrations of the (Na, Bi) and (K, Bi) ions in the NaBTi and the KBTi thin films, respectively. The formation of the Raman modes above  $200$   $cm^{-1}$  can be related to the bending, rotating, tilting, and stretching vibrations of the  $TiO_6$  octahedra [22]. The formation of intense peaks at  $270$   $cm^{-1}$  for the NaBTi and  $269$   $cm^{-1}$  for the KBTi can be related to the torsional bending vibrations of the  $TiO_6$  octahedra. The phonon modes above  $500$   $cm^{-1}$  in the NaBTi and the KBTi thin films can be attributed to the stretching vibrations of the  $TiO_6$  octahedra in the pseudo-perovskite block [22]. The formation of an intense peak at  $\sim 850$   $cm^{-1}$  can be related to the symmetric stretching of the  $TiO_6$  octahedra [21, 22].

From Fig. 2, it is obvious that doping of the Bi-site of the NaBTi and the KBTi thin films with  $Sm^{3+}$ -ions leads to few visible changes in the Raman spectra of the NaBSmTi and the KBSmTi thin films. The broad split modes, which were observed at  $559$   $cm^{-1}$  and  $623$   $cm^{-1}$  in the NaBTi thin film, were observed as intense modes with a slight shift in the NaBSmTi thin film. In the same manner, some changes were observed in the KBSmTi thin film at frequencies of  $576$   $cm^{-1}$  and  $621$   $cm^{-1}$  compared to the KBTi thin film. Furthermore, in both NaBSmTi and KBSmTi thin films, the phonon modes in the low-frequency region softened compared to the NaBTi and the KBTi thin films. Changes in the Raman spectra of the thin film can be related to the structural disorder caused by doping the heavier  $Sm^{3+}$ -ion into the Bi-site of the  $M_{0.5}Bi_{4.5-x}Sm_xTi_4O_{15}$  ( $M = Na$  or  $K$ ) thin films [22]. The internal strain induced by the  $Sm^{3+}$ -ion doping, which is caused by ionic radius difference between  $Sm^{3+}$ - and  $Bi^{3+}$ -ions, is responsible for the observed Raman spectra changes of both NaBSmTi and KBSmTi films [20, 22].

The effects of  $Sm^{3+}$ -ion doping on the microstructure of the films were examined using FE-SEM analysis. Both surface morphologies and cross-sectional micrographs of the  $M_{0.5}Bi_{4.5-x}Sm_xTi_4O_{15}$  ( $x = 0$  and  $0.5$ ,  $M = Na$  or  $K$ )

**Table 1.** Assignments of the Raman active modes for the NaBTi, KBTi, NaBSmTi, and KBSmTi thin films.

Thin films	Raman frequencies ( $cm^{-1}$ )									
NaBTi	124	153	213	270	323	385	–	559	623	850
NaBSmTi	126	152	208	268	317	344	538	558		852
KBTi	123	147	183	223	269	332	548	576	621	847
KBSmTi	123	146	180	220	266	331	3.2 cm	568	616	850

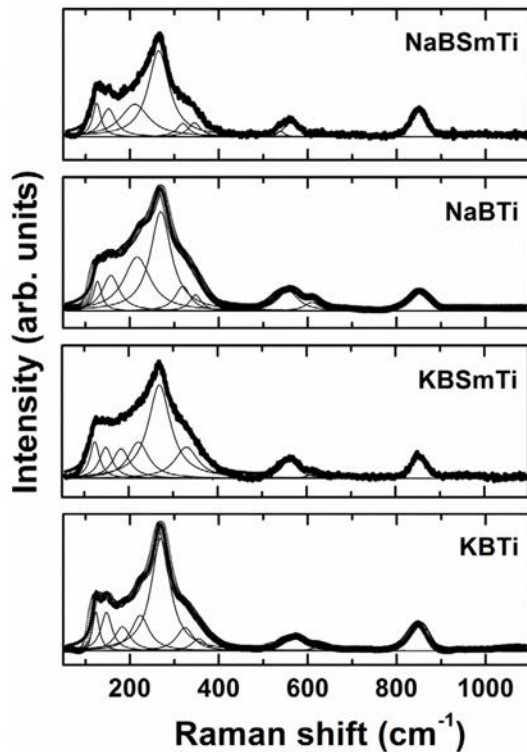


**Fig. 3.** SEM surface morphologies with cross-sectional micrographs of the NaBTi, KBTi, NaBSmTi, and KBSmTi thin films.

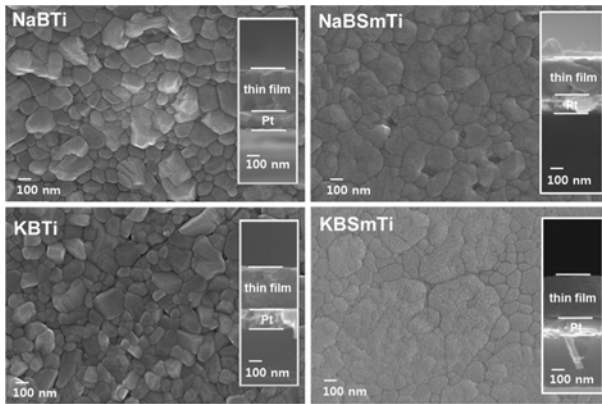


**Fig. 4.** (a) Leakage current densities of the NaBTi, KBTi, NaBSmTi, and KBSmTi thin films and (b) the  $\log(J)$ - $\log(E)$  characteristics for understanding the leakage current mechanisms.

films are shown in Fig. 3. From the surface images, films were filled with grains with different grain sizes without any major cracks. The grains in all the thin films were found to have an uneven distribution in their size. As seen in the figure, the grains of the NaBTi and the KBTi thin films exhibited irregular brick-like morphologies. The  $\text{Sm}^{3+}$ -ion doping significantly affects the grain growth of the NaBTi and the KBTi thin films. Furthermore, clearly different surface morphologies (island-like morphologies) were found in the NaBSmTi and the KBSmTi thin films. The thicknesses of the films were found to be approximately 300 nm as

shown in the Fig. 3.

Leakage current behaviors of the films were investigated to study the  $\text{Sm}^{3+}$ -ion. The leakage current densities with various applied electric fields are shown in Fig. 4(a). It is obvious that  $\text{Sm}^{3+}$ -ions doping on the Bi-site of the  $M_{0.5}\text{Bi}_{4.5}\text{Ti}_4\text{O}_{15}$  ( $M = \text{Na}$  or  $\text{K}$ ) significantly lowers the leakage current density of the  $M_{0.5}\text{Bi}_{4.5-x}\text{Sm}_x\text{Ti}_4\text{O}_{15}$  thin films. At applied electric field of 100 kV/cm, the leakage current densities of the NaBTi, NaBSmTi, KBTi, and KBSmTi thin films were  $7.38 \times 10^{-6}$ ,  $1.11 \times 10^{-7}$ ,  $5.74 \times 10^{-7}$ , and  $4.65 \times 10^{-8}$  A/cm<sup>2</sup>, respectively. Low leakage current densities observed for the  $M_{0.5}\text{Bi}_{4.5-x}\text{Sm}_x\text{Ti}_4\text{O}_{15}$  thin films can be correlated to the reduced concentration of oxygen vacancies caused by the  $\text{Sm}^{3+}$ -ion doping. The lowest leakage current density was found from the KBSmTi thin film.

To investigate the leakage current mechanisms, logarithmic plots of the leakage current densities vs. the applied electric field were shown in Fig. 4(b). All the thin films obey the Ohmic conduction mechanism in the low electric field region, which is evident from the slope,  $S \sim 1$ . Primarily, in ferroelectric thin films, the Ohmic conduction mechanism is caused by the flow of thermally injected electrons [23]. With a larger electric field than 130 kV/cm, the NaBTi film exhibits slope value of  $S \sim 3$ , which suggests a new conduction mechanism of space charge limited (SCL) conduction combined with other unknown conduction mechanisms (Child law) [23, 24]. The leakage current caused by the SCL conduction in the high electric field region is mainly due to the flow of free charge carriers. On the other hand, the NaBSmTi thin film showed an Ohmic conduction mechanism over the entire region of the applied electric field. For the KBTi thin film, the Ohmic conduction mechanism dominated until 85 kV/cm, above which the applied electric field led to a sudden increase in the leakage current with a slope,  $S > 4$ . The formation of this slope described the trap-filled limited (TFL) conduction mechanism, in which the leakage current is mainly caused by the flow of excess charges, which remain after filling all available traps in the thin film [23, 24]. The TFL conduction mechanism was dominant until 125 kV/cm in the KBTi thin film. In the high electric field region, the value of the slope was estimated to be  $\sim 3$ , indicating SCL conduction with other unknown conduction mechanisms. The triangle formed by the slopes of three distinct regions in the KBTi thin film is named Lambert's triangle [24]. Different conduction behavior was observed for the KBSmTi thin film, in that, above 90 kV/cm, the conduction mechanism changed from Ohmic ( $S \sim 1$ ) to an SCL conduction mechanism ( $S \sim 2$ ), which was dominant until 150 kV/cm. The applied electric field above 150 kV/cm led to the observation of the TFL conduction mechanism ( $S > 4$ ) with a sudden increase of current in the KBSmTi thin film.

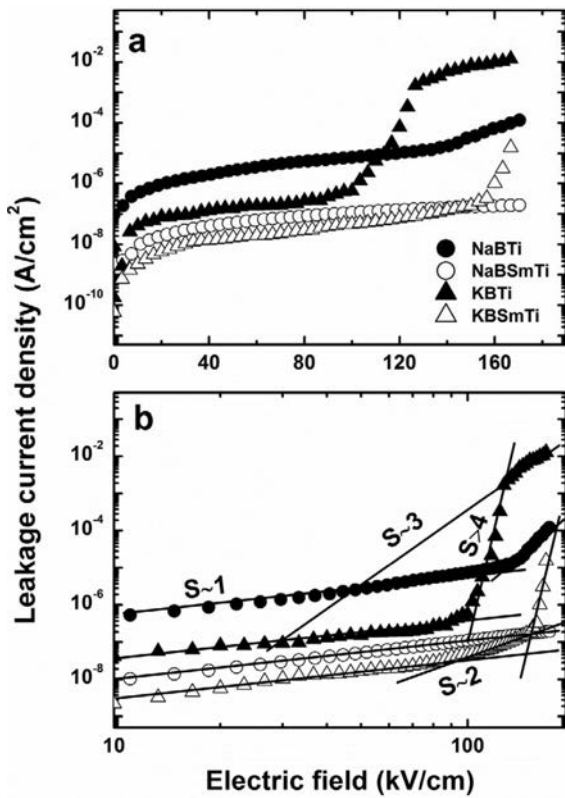


Fig. 5. Frequency-dependent dielectric properties of the NaBTi, KBTi, NaBSmTi, and KBSmTi thin films.

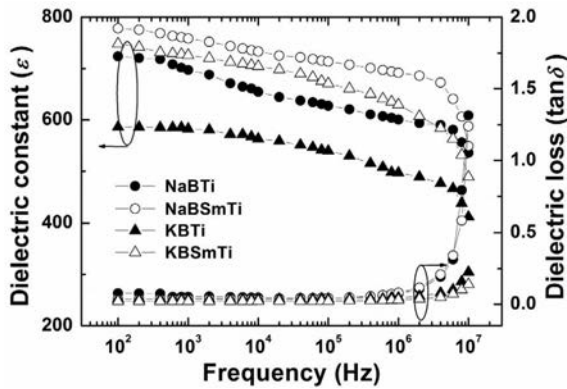


Fig. 6. Ferroelectric polarization-electric field ( $P$ - $E$ ) hysteresis loops of the NaBTi, KBTi, NaBSmTi, and KBSmTi thin films.

The dielectric properties of the thin films were measured at room temperature and are shown in Fig. 5. The dielectric constants and the dielectric losses of the thin films were measured at the frequency ranges of  $10^2$  to  $10^7$  Hz. From Fig. 5, it is obvious that doping the Bi-site with  $Sm^{3+}$  ions can potentially improve the dielectric properties of the NaBSmTi and the KBSmTi thin films. The dielectric constant ( $\epsilon$ ) and dielectric loss values for the NaBTi, NaBSmTi, KBTi, and KBSmTi thin films at 1 kHz were 697 and 0.050, 758 and 0.038, 582 and 0.036, and 726 and 0.021, respectively. The dielectric loss in a ferroelectric thin film can be directly

related to the space charge components, caused by the oxygen vacancies [25]. The presence of an increased number of oxygen vacancies leads to an increase in dielectric loss in ferroelectric thin films [25]. Therefore, the low dielectric loss values observed for the NaBSmTi and the KBSmTi thin films can be attributed to the presence of a low concentration of oxygen vacancies caused by the  $Sm^{3+}$ -ion doping of the Bi-site of the  $M_{0.5}Bi_{4.5}Ti_4O_{15}$  ( $M = Na$  or  $K$ ) thin films.

The ferroelectricity of the thin films was investigated by measuring the ferroelectric polarization-electric field ( $P$ - $E$ ) hysteresis loops at a frequency of 1.25 kHz using triangular pulses at room temperature as shown in Fig. 6. From Fig. 6, it is obvious that well-defined ferroelectric  $P$ - $E$  hysteresis loops with significantly enhanced remnant polarization values were observed for the  $Sm^{3+}$ -ion doped NaBSmTi and KBSmTi thin films. The remnant polarization ( $2P_r$ ) and the coercive electric field ( $2E_c$ ) values of the NaBTi and the NaBSmTi thin films were measured to be 13.1  $\mu C/cm^2$  and 308 kV/cm and 34.4  $\mu C/cm^2$  and 220 kV/cm at an electric field of 475 kV/cm, respectively. On the other hand, the  $2P_r$  and the  $2E_c$  values of the KBTi and the KBSmTi thin films were measured to be 13.3  $\mu C/cm^2$  and 149 kV/cm and 36.0  $\mu C/cm^2$  and 103 kV/cm at an electric field of 231 kV/cm, respectively. Memory devices preferably require ferroelectric thin films to display the following properties: a large remnant polarization and low coercive electric field. It is interesting to note that the incorporation of  $Sm^{3+}$  ions into the Bi-site of the  $M_{0.5}Bi_{4.5}Ti_4O_{15}$  has the effect of drastically reducing the coercive electric field exhibited by these compounds. The improved ferroelectric properties of the NaBSmTi and the KBSmTi thin films can be well correlated with the decrease in the leakage current density of both films. The suppression of electrical conduction, which is caused by doping the Bi-sites of NaBTi and KBTi with  $Sm^{3+}$  ions, favors an increase in the number of available ferroelectric switching domains by decreasing the number of oxygen vacancies. The presence of excessive oxygen vacancies leads to domain pinning at domain boundaries, which is capable of preventing domain switching in ferroelectric thin films [20, 26]. Furthermore, the strain generated by the incorporation of the heavier  $Sm^{3+}$ -ion may induce local lattice distortion, which would favor an increase in ferroelectric polarization in the NaBSmTi and the KBSmTi thin films [2, 20].

## Conclusions

In summary, the  $Sm^{3+}$ -ion doped  $M_{0.5}Bi_{4.5-x}Sm_xTi_4O_{15}$  ( $x = 0$  and  $0.5$ ,  $M = Na$  or  $K$ ) thin films were prepared on Pt(111)/Ti/SiO<sub>2</sub>/Si(100) substrates by using a CSD technique. Fabricated films were crystallized in Aurivillius phase orthorhombic structures without any traces of secondary or impurity phases. Doping with

Sm<sup>3+</sup>-ions resulted in a low leakage current density, low dielectric loss, large ferroelectric polarization, and low coercive electric field for the  $M_{0.5}Bi_{4.5-x}Sm_xTi_4O_{15}$  thin films. The stable Aurivillius structure with a reduced concentration of ionic defects, such as bismuth and oxygen vacancies, and the local lattice distortion induced by doping the Bi-sites of the NaBTi and the KBTi thin films with Sm<sup>3+</sup>-ions can explain the enhanced electrical and ferroelectric properties of the NaBSmTi and the KBSmTi thin films. This study indicates that it is plausible to recommend Sm<sup>3+</sup>-doping as a way of enhancing the remnant polarization and reducing the coercive electric field of the BLSF thin films. Furthermore, the results observed for these thin films show that they are highly attractive for use in ferroelectric applications.

### Acknowledgments

This research was supported by Basic Science Research Program through the National Research Foundation of Korea (NRF) funded by the Ministry of Education, Science and Technology (2011-0030058). W. J. Kim appreciates the partial financial support from Changwon National University (2017).

### References

1. C.A. Araujo, J.D. Cuhairo, L.D. McMillan, et al, Nature 374 (1995) 627-629.
2. U. Chon, H.M. Jang, M.G. Kim, et. al, Phys. Rev. Lett. 89 (2002) 087601.
3. H. Irie, M. Miyayama, T. Kudo, J. Appl. Phys. 90 (2001) 4089-4094.
4. C.-M. Wang, L. Zhao, J.-F. Wang, et. al, T.R. Shrout, Phys. Status Solidi RRL 3 (2009) 7-9.
5. C.-M. Wang, J.-F. Wang, J. Am. Ceram. Soc. 91 (2008) 918-923.
6. L. Keeney, T. Maity, M. Schmidt, A. Amann, et al, J. Am. Ceram. Soc. 96 (2013) 2339-2357.
7. E.C. Subbarao, J. Phys. Chem. Solids 23 (1962) 665-676.
8. M.L. Calzada, R. Jiménez, A. González, et. al, Chem. Mater. 13 (2001) 3-5.
9. B.H. Park, B.S. Kang, S.D. Bu, T.W. et al, Nature 401 (1999) 682-684.
10. Y. Noguchi, M. Suzuki, Y. Kitanaka, et. al, Appl. Phys. Lett. 93 (2008) 032904.
11. Z.X. Cheng, X.L. Wang, H.Y. Zhao, et al, J. Appl. Phys. 107 (2010) 084105.
12. X.-P. Jiang, X.-L. Fu, C. Chen, et. al, J. Adv. Ceram. 4 (2015) 54-60.
13. H. Du, X. Shi, J. Phys. Chem. Solids 72 (2011) 1279-1283.
14. S. Ikegami, I. Ueda, Jpn. J. Appl. Phys. 13 (1974) 1572-1577.
15. C.-M. Wang, J.-F. Wang, S. Zhang, et. al, J. Appl. Phys. 105 (2009) 094110.
16. D. Gao, K.W. Kwok, D. Lin, Curr. Appl. Phys. 11 (2011) S124-S127.
17. D.H. Kang, Y.H. Kang, J. Microelectronics Packaging Soc. 20 (2013) 25-30.
18. U. Chon, K.B. Kim, H.M. Jang, et. al, Appl. Phys. Lett. 79 (2001) 3137-3139.
19. M. Chen, Z.L. Liu, Y. Wang, et. al, Physica B 352 (2004) 61-65.
20. C. Long, Q. Chang, Y. Wu, et. al, J. Mater. Chem. C 3 (2015) 8852-8864.
21. S. Kojima, R. Imaizumi, S. Hamazaki, et al, J. Mol. Struct. 348 (1995) 37-40.
22. H. Hao, H.X. Liu, M.H. Cao, et. al, Appl. Phys. A 85 (2006) 69-73.
23. C. Wang, M. Takahashi, H. Fujino, X. Zhao, E. Kume, T. Horiuchi, S. Sakai, J. Appl. Phys. 99 (2006) 054104.
24. A. Roy, S. Maity, A. Dhar, D. Bhattacharya, S.K. Ray, J. Appl. Phys. 105 (2009) 044103.
25. I. Coondoo, A.K. Jha, S.K. Agarwal, Ceram. Int. 33 (2007) 41-47.
26. J.F. Scott, C.A. Paz de Araujo, B.M. Melnick, L.D. McMillan, R. Zuleeg, J. Appl. Phys. 70 (1991) 382-388.